# Chapter 4

# Deployment Strategies of Multiple Reconfigurable Intelligent Surface Assisted Downlink NOMA System*

*Part of this work has been published as:

**M. Hemanta Kumar**, Sanjeev Sharma, Kuntal Deka, and M. Thottappan. "Centralized and Distributed Reconfigurable Intelligent Surfaces Assisted NOMA", *2022 National Conference on Communications (NCC).* IEEE, 2022

**M. Hemanta Kumar**, Sanjeev Sharma, Kuntal Deka, and M. Thottappan. "Multiple Reconfigurable Intelligent Surfaces Assisted Downlink NOMA System", *International Journal of Communication Systems - Wiley.* 2022; doi: 10.1002/dac.5287.

## 4.1 Introduction

In this chapter, the focus is mainly on the deployment of RISs under the path loss component and the creation of a virtual LoS path between the base station and users. Initially, two different deployment strategies of RIS-assisted precoded NOMA for the downlink multiple-input and single-output (MISO) system is considered. The BS consists of multiple antennas and users use a single antenna. Firstly, RISs are placed near to each user, which is called distributed RIS deployment. In the second method, a single RIS is deployed at the BS, which is called centralized RIS deployment.

A single RIS is insufficient to create a LoS path between the BS and users in a high scattering environment. Further, path losses are higher in millimeter and terahertz frequencies than sub-GHz bands due to molecular absorption. Moreover, cell-edge NOMA users suffer high attenuation [92]. To address the issues mentioned above, we consider multiple RIS (MRIS) to establish LoS paths between BS and the users. The LoS path improves the wireless network's performance, especially in higher frequency bands and severe path blockage scenarios. MRISs use multihop reflections to serve users in a system with virtual LoS paths, which results in improved performance. Therefore, multiple RISs-assisted NOMA systems are proposed and analyzed, especially for millimeter and terahertz bands communication systems.

The main contributions of the chapter are summarized as to follows:

- The BER performance is analyzed for both distributed and centralized RIS-assisted NOMA by using the phase optimization of reflecting elements through the semidefinite relaxation (SDR) method.

- The sum-rate of the proposed NOMA system is also calculated. The BER and sum-rate performances of centralized deployment are better than the distributed deployment of RISs for the total fixed surfaces.

- Further, the sum-rate of the proposed system is better than conventional OMA like time division multiple access (TDMA) and frequency division multiple access (FDMA) systems.

- The impact of transmitting antennas at the BS and reflecting surfaces at RIS is studied by varying the RIS positions in the proposed system.

- A mathematical expression for bit error probability (BEP) under Rician fading channels with path loss components is derived, and verified numerically.

- The simulation results show that the p[roposed system achieved low BEP at low transmit power, and improved the cell-edge users' performance due to multiple RISs, which reconfigure the propagation environment and create a virtual multiple-input multiple-output (MIMO) system among the RISs.

- Impact of the positions of RIS panels, the number of reflecting surfaces, the number of RISs, imperfect SIC, and the power of the LoS path, is analyzed on BEP performance in the proposed multiple RIS assisted NOMA system.

- The BEP is also simulated in the Rician fading channel scenario and compared with Rayleigh fading channel. Furthermore, the proposed system is analyzed for different order modulation schemes.

- Finally, the performance of proposed multiple RIS assisted NOMA system system's is compared with existing RIS-NOMA and parallel MRIS-assisted systems.

This chapter is organized as follows. In Section 4.2 & 4.4 , the proposed multiple RIS-assisted NOMA and deployment strategies are presented. Analytical expressions of the near and far users in Section 4.5. Analytical and simulation results are presented in Section 4.3 &4.6 . the summary is of the chapter is made in Sections 4.7.

## 4.2 Proposed RIS-assisted NOMA System Model

We consider two distributed and centralized RIS deployment strategies in the proposed NOMA system.

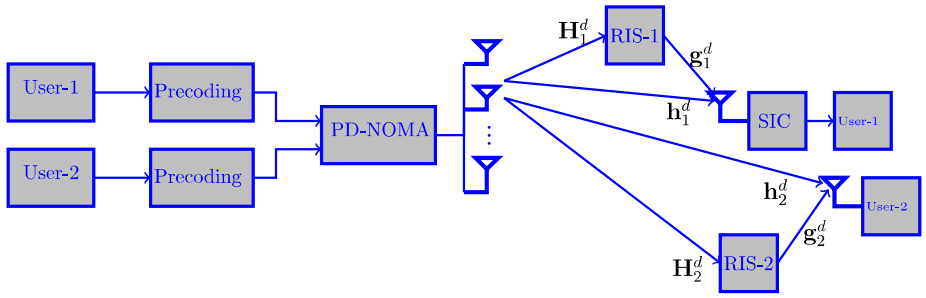


[a] Distributed deployment

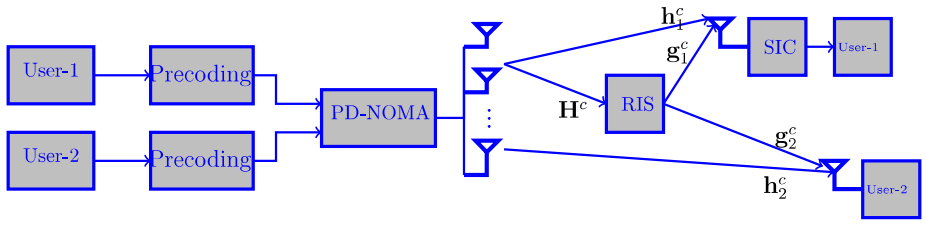


[b] Centralized deployment

FIGURE 4.1: RIS-assisted NOMA system

### 4.2.1 Distributed RIS-assisted NOMA System

The block diagram of distributed RIS assisted NOMA system (DDR-NOMA) for downlink MISO system is shown in Figure4.1 [a], where the BS is equipped with $N_{\mathrm{t}}$ transmit antennas. The BS transmits superimposed symbols to near user (NU) $\mathcal{U}_1$ and far user (FU) $\mathcal{U}_2$. Both NU and FU are equipped with a single antenna. Further, RIS-1 and RIS-2 are deployed near to $\mathcal{U}_1$ and $\mathcal{U}_2$, respectively. RIS-1 and RIS-2 consist of $N_1$ and $N_2$ passive reflecting surfaces, respectively. Moreover, channel between BS and RIS-1 is considered as $\mathbf{H}_1^{\mathrm{d}} \in \mathbb{C}^{N_1 \times N_{\mathrm{t}}}$ and BS and RIS-2 is considered as $\mathbf{H}_2^{\mathrm{d}} \in \mathbb{C}^{N_2 \times N_{\mathrm{t}}}$ follows the Rician distribution which are given as

$$\mathbf{H}_1^{\mathrm{d}} = \frac{1}{\sqrt{d_{\mathrm{BR_1}}^{\beta}}} \left( \sqrt{\frac{\mathrm{K}_1^{\mathrm{d}}}{\mathrm{K}_1^{\mathrm{d}}+1}} \tilde{\mathbf{H}}_1^{\mathrm{d}} + \sqrt{\frac{1}{\mathrm{K}_1^{\mathrm{d}}+1}} \bar{\mathbf{H}}_1^{\mathrm{d}} \right) \in \mathbb{C}^{N_1 \times N_{\mathrm{t}}}, \tag{4.1}$$

and

$$\mathbf{H}_2^{\mathrm{d}} = \frac{1}{\sqrt{d_{\mathrm{BR_2}}^{\beta}}} \left( \sqrt{\frac{\mathrm{K}_2^{\mathrm{d}}}{\mathrm{K}_2^{\mathrm{d}}+1}} \tilde{\mathbf{H}}_2^{\mathrm{d}} + \sqrt{\frac{1}{\mathrm{K}_2^{\mathrm{d}}+1}} \bar{\mathbf{H}}_2^{\mathrm{d}} \right) \in \mathbb{C}^{N_2 \times N_{\mathrm{t}}}, \tag{4.2}$$

where, $d_{\mathrm{BR_1}}$ and $d_{\mathrm{BR_2}}$ are distances between the BS and RIS-1, and BS and RIS-2, respectively, $\beta$ represents the path loss exponent. The $\tilde{\mathbf{H}}_1^{\mathrm{d}}$ and $\tilde{\mathbf{H}}_2^{\mathrm{d}}$ denote the line-of-sight (LoS) components, and $\bar{\mathbf{H}}_1^{\mathrm{d}}$ and $\bar{\mathbf{H}}_2^{\mathrm{d}}$ represent non-LoS (NLoS) components with Rayleigh flat fading and $\mathrm{K}_1^{\mathrm{d}}$ and $\mathrm{K}_2^{\mathrm{d}}$ are Rician factors. Similarly, the channel vectors between RIS-1 and $\mathcal{U}_1$ and RIS-2 and $\mathcal{U}_2$, are $\mathbf{g}_1^{\mathrm{d}}$ and $\mathbf{g}_2^{\mathrm{d}}$ respectively, which are Rician distributed as follows,

$$\mathbf{g}_1^{\mathrm{d}} = \frac{1}{\sqrt{d_{\mathrm{R_1U_1}}^{\beta}}} \sqrt{\frac{\mathrm{K}_{11}^{\mathrm{d}}}{\mathrm{K}_{11}^{\mathrm{d}}+1}} \tilde{\mathbf{g}}_1^{\mathrm{d}} + \sqrt{\frac{1}{\mathrm{K}_{11}^{\mathrm{d}}+1}} \bar{\mathbf{g}}_1^{\mathrm{d}} \in \mathbb{C}^{N_1 \times 1}, \tag{4.3}$$

and

$$\mathbf{g}_2^{\mathrm{d}} = \frac{1}{\sqrt{d_{\mathrm{R_2U_2}}^{\beta}}} \sqrt{\frac{\mathrm{K}_{22}^{\mathrm{d}}}{\mathrm{K}_{22}^{\mathrm{d}}+1}} \tilde{\mathbf{g}}_2^{\mathrm{d}} + \sqrt{\frac{1}{\mathrm{K}_{22}^{\mathrm{d}}+1}} \bar{\mathbf{g}}_2^{\mathrm{d}} \in \mathbb{C}^{N_2 \times 1}, \tag{4.4}$$

where, $\tilde{\mathbf{g}}_1^{\mathrm{d}}$ and $\tilde{\mathbf{g}}_2^{\mathrm{d}}$ are the LoS $\bar{\mathbf{g}}_1^{\mathrm{d}}$, and $\bar{\mathbf{g}}_2^{\mathrm{d}}$ are NLoS components with Rayleigh flat fading, $\mathrm{K}_{11}^{\mathrm{d}}$ and $\mathrm{K}_{11}^{\mathrm{d}}$ are Rician factors, $d_{\mathrm{R_1U_1}}$ and $d_{\mathrm{R_2U_2}}$ denote the distance between RIS-1 and $\mathcal{U}_1$ and RIS-2 and $\mathcal{U}_2$.

The direct links between the BS and users $\mathcal{U}_1$ and $\mathcal{U}_2$ exist and are denoted by $\mathbf{h}_1^{\mathrm{d}} \in \mathbb{C}^{N_{\mathrm{t}} \times 1}$ and $\mathbf{h}_2^{\mathrm{d}} \in \mathbb{C}^{N_{\mathrm{t}} \times 1}$ respectively, which are considered Rayleigh-flat fading and independent and identical distributed (iid) with $\mathbf{h}_{\mathrm{v}}^{\mathrm{d}} \sim \mathcal{CN}(0, \sigma_{\mathrm{v}}^2)$, $\mathrm{v} = 1, 2$. The NU and FU distances from the BS are $d_{\mathrm{B}_1}$ and $d_{\mathrm{B}_2}$, respectively. Let $\eta$ be the path loss component of the direct link, and the channel gain of $\mathcal{U}_1$ is higher than $\mathcal{U}_2$.
In DDR-NOMA system, the BS transmits the superimposed precoded symbols of $\mathcal{U}_1$ and $\mathcal{U}_2$ as shown in Figure 4.1, and the received signal at user $\mathcal{U}_1$ is expressed as,

$$y_1^{\mathrm{d}} = \mathbf{f}_1^{\mathrm{d}} \left( \mathbf{w}_1^{\mathrm{d}} \sqrt{\alpha_1 \mathrm{P}} x_1 + \mathbf{w}_2^{\mathrm{d}} \sqrt{(1-\alpha_1)\mathrm{P}} x_2 \right) + n_1^{\mathrm{d}}, \tag{4.5}$$

where, $x_1$ and $x_2$ denote the binary phase shift keying (BPSK) symbols. The $\alpha_1$ and $(1-\alpha_1)$ are power coefficients assigned to $\mathcal{U}_1$ and $\mathcal{U}_2$ according to their channel gains and P is the total transmitted power available at the BS. Further, $\mathbf{f}_1^{\mathrm{d}} = \left( \mathbf{g}_1^{\mathrm{d}H} \mathbf{\Phi}_1^{\mathrm{d}} \mathbf{H}_1^{\mathrm{d}} + \mathbf{h}_1^{\mathrm{d}H} \right)$ whichis an effective channels between the BS and $\mathcal{U}_1$, where $\mathbf{\Phi}_1^{\mathrm{d}} \in \mathbb{C}^{N_1 \times N_1}$ is a diagonal matrix which is given as $\mathbf{\Phi}_1^{\mathrm{d}} = \mathrm{diag}[A_1 \mathrm{e}^{\phi_1}, A_2 \mathrm{e}^{\phi_2}, \ldots, A_{N_1} \mathrm{e}^{\phi_{N_1}}]$, where $A_n \in (0, 1]$ denotes the reflecting coefficients, and in general $|A_n| = 1 \ \forall n$, and $\mathbf{w}_1^{\mathrm{d}}$ and $\mathbf{w}_2^{\mathrm{d}}$ are a zero-forcing precoders, which provide an optimal beamforming [93]. The beamforming vectors are expressed as,

$$\mathbf{w}_1^{\mathrm{d}} = \frac{\mathbf{f}_1^{\mathrm{d}H} (\mathbf{f}_1^{\mathrm{d}} \mathbf{f}_1^{\mathrm{d}H})^{-1}}{\left\| \mathbf{f}_1^{\mathrm{d}} \left( \mathbf{f}_1^{\mathrm{d}} \mathbf{f}_1^{\mathrm{d}H} \right)^{-1} \right\|_2^2} \in \mathbb{C}^{N_{\mathrm{t}} \times 1}, \tag{4.6}$$

and

$$\mathbf{w}_2^{\mathrm{d}} = \frac{\mathbf{f}_2^{\mathrm{d}H} (\mathbf{f}_2^{\mathrm{d}} \mathbf{f}_2^{\mathrm{d}H})^{-1}}{\left\| \mathbf{f}_2^{\mathrm{d}} (\mathbf{f}_2^{\mathrm{d}} \mathbf{f}_2^{\mathrm{d}H})^{-1} \right\|_2^2} \in \mathbb{C}^{N_{\mathrm{t}} \times 1}. \tag{4.7}$$

Similarly, the received signals at user $\mathcal{U}_2$ is

$$y_2^{\mathrm{d}} = \mathbf{f}_2^{\mathrm{d}} \left( \mathbf{w}_1^{\mathrm{d}} \sqrt{\alpha_1 \mathrm{P}} x_1 + \mathbf{w}_2^{\mathrm{d}} \sqrt{(1-\alpha_1)\mathrm{P}} x_2 \right) + n_2^{\mathrm{d}}, \tag{4.8}$$

where, $\mathbf{f}_2^{\mathrm{d}} = \left( \mathbf{g}_2^{\mathrm{d}H} \mathbf{\Phi}_2^{\mathrm{d}} \mathbf{H}_2^{\mathrm{d}} + \mathbf{h}_2^{\mathrm{d}H} \right)$ denotes an effective channel between the BS and $\mathcal{U}_2$, where $\mathbf{\Phi}_2^{\mathrm{d}} \in \mathbb{C}^{N_2 \times N_2}$ is a diagonal matrix which is given as $\mathbf{\Phi}_2^{\mathrm{d}} = \mathrm{diag}[A_1 \mathrm{e}^{\phi_1}, A_2 \mathrm{e}^{\phi_2}, \ldots, A_{N_2} \mathrm{e}^{\phi_{N_2}}]$ and $n_v^{\mathrm{d}}, v = 1, 2$ denotes the white Gaussian noise with $\sim \mathcal{CN}(0, N_0)$.

### 4.2.2 Detection of DDR-NOMA Users

The NU uses SIC for signal detection in which first removes the interference signal of $\mathcal{U}_2$ from the received signal, after that it applies maximum likely-hood (ML) detector. Moreover, symbols of FU are decoded directly from the received signal by using the ML detector.

The ML detection of $\mathcal{U}_2$ at the NU is expressed as

$$\hat{x}_2^{\mathrm{NU}} = \arg\min_{x_2} \left\| y_1^{\mathrm{d}} - \mathbf{f}_1^{\mathrm{d}} \left( \mathbf{w}_1^{\mathrm{d}} \sqrt{\alpha_1 \mathrm{P}} x_1 + \mathbf{w}_2^{\mathrm{d}} \sqrt{(1-\alpha_1)\mathrm{P}} x_2 \right) \right\|_2^2. \tag{4.9}$$

The SIC subtracts interference symbols $\hat{x}_2^{\mathrm{NU}}$ from the received signals $y_1$ which is given as,

$$y_1^{\mathrm{SIC}} = y_1^{\mathrm{d}} - \left[ \mathbf{f}_1^{\mathrm{d}} \left( \mathbf{w}_2^{\mathrm{d}} \sqrt{(1-\alpha_1)\mathrm{P}} \right) \hat{x}_2^{NU} \right]. \tag{4.10}$$

Therefore, the symbols of NU's are extracted using the ML detector after applying the SIC, which is given as,

$$\hat{x}_1 = \arg\min\nolimits_{x_1} \left\| y_1^{\mathrm{SIC}} - \mathbf{f}_1^{\mathrm{d}} \left( \mathbf{w}_1^{\mathrm{d}} \sqrt{\alpha_1 \mathrm{P}} x_1 + \mathbf{w}_2^{\mathrm{d}} \sqrt{(1-\alpha_1)\mathrm{P}} x_2 \right) \right\|_2^2. \tag{4.11}$$

The FU symbols are decoded directly by using ML decoder as,

$$\hat{x}_2 = \arg\min_{x_2} \left\| y_2^{\mathrm{d}} - \mathbf{f}_1^{\mathrm{d}} \left( \mathbf{w}_1^{\mathrm{d}} \sqrt{\alpha_1 \mathrm{P}} x_1 + \mathbf{w}_2^{\mathrm{d}} \sqrt{(1-\alpha_1)\mathrm{P}} x_2 \right) \right\|_2^2. \tag{4.12}$$

### 4.2.3 SNR Optimization through Distributed Algorithm

The SNR at the NU is expressed after perfect SIC as,

$$\gamma^{\mathrm{NU_d}} = \frac{\left| \left( \mathbf{g}_1^{\mathrm{d}H} \mathbf{\Phi}_1^{\mathrm{d}} \mathbf{H}_1^{\mathrm{d}} + \mathbf{h}_1^{\mathrm{d}H} \right) \mathbf{w}_1^{\mathrm{d}} \right|^2 \alpha_1 \mathrm{P}}{N_0}. \tag{4.13}$$

The SNR of the NU is maximized by optimizing the phase shift matrix for a given transmit beamforming $\mathbf{w}_1^{\mathrm{d}}$ as,

$$\begin{aligned} (\mathrm{PO}) : & \max_{\mathbf{\Phi}_1^{\mathrm{d}}} \left| \left( \mathbf{g}_1^{\mathrm{d}H} \mathbf{\Phi}_1^{\mathrm{d}} \mathbf{H}_1^{\mathrm{d}} + \mathbf{h}_1^{\mathrm{d}H} \right) \mathbf{w}_1^{\mathrm{d}} \right|^2 \\ & \text{s.t. } 0 \leq \phi_{1,n} \leq 2\pi, \forall n. \end{aligned} \tag{4.14}$$

Recall $\mathbf{\Phi}_1^{\mathrm{d}}$ is $\mathbf{\Phi}_1^{\mathrm{d}} = \mathrm{diag}[\mathrm{e}^{\phi_{1,1}}, \ldots, \mathrm{e}^{\phi_{1,n}}, \ldots, \mathrm{e}^{\phi_{1,N_1}}]$. The above (PO) problem holds the following inequality, since it is a non-convex

$$\begin{aligned} |(\mathbf{g}_1^{\mathrm{d}H} \mathbf{\Phi}_1^{\mathrm{d}} \mathbf{H}_1^{\mathrm{d}} + \mathbf{h}_1^{\mathrm{d}H}) \mathbf{w}_1^{\mathrm{d}}| &= |\mathbf{g}_1^{\mathrm{d}H} \mathbf{\Phi}_1^{\mathrm{d}} \mathbf{H}_1^{\mathrm{d}} \mathbf{w}_1^{\mathrm{d}} + \mathbf{h}_1^{\mathrm{d}H} \mathbf{w}_1^{\mathrm{d}}| \\ &\overset{(q)}{\leq} |\mathbf{g}_1^{\mathrm{d}H} \mathbf{\Phi}_1^{\mathrm{d}} \mathbf{H}_1^{\mathrm{d}} \mathbf{w}_1^{\mathrm{d}}| + |\mathbf{h}_1^{\mathrm{d}H} \mathbf{w}_1^{\mathrm{d}}|. \end{aligned} \tag{4.15}$$

In $(q)$ equality holds if and only if $\arg(\mathbf{g}_1^{\mathrm{d}H} \mathbf{\Phi}_1^{\mathrm{d}} \mathbf{H}_1^{\mathrm{d}} \mathbf{w}_1^{\mathrm{d}}) = \arg(\mathbf{h}_1^{\mathrm{d}H} \mathbf{w}_1^{\mathrm{d}}) \triangleq \theta_0$. Further, solution of $\boldsymbol{\phi}_1$ and phase constraints in (4.14) are satisfied with in equality $(q)$. Let, $\mathbf{g}_1^{\mathrm{d}H} \mathbf{\Phi}_1^{\mathrm{d}} \mathbf{H}_1^{\mathrm{d}} \mathbf{w}_1^{\mathrm{d}} = \mathbf{m}^H \mathbf{q}$, where $\mathbf{q} = \mathrm{diag}(\mathbf{g}_1^{\mathrm{d}H}) \mathbf{H}_1^{\mathrm{d}} \mathbf{w}_1^{\mathrm{d}}$ and $\mathbf{m} = [\mathrm{e}^{\phi_{1,1}}, \ldots, \mathrm{e}^{\phi_{1,n}}, \ldots, \mathrm{e}^{\phi_{1,N_1}}]^H$.

However, the optimization problem (PO) is equivalent to

$$(\text{PO}'): \quad \max_{\mathbf{m}} \quad |\mathbf{m}^H \mathbf{q}| \tag{4.16}$$

$$\text{s.t.} \quad |m_n| = 1,\ n = 1,\ \cdots,\ N_1, \tag{4.17}$$

$$\arg(\mathbf{m}^H \mathbf{q}) = \theta_0. \tag{4.18}$$

Therefore, the optimal solution of (PO$'$) is given as,

$$\mathbf{m}^* = \mathrm{e}^{j(\theta_0 - \arg(\mathbf{q}))} = \mathrm{e}^{j(\theta_0 - \arg(\mathrm{diag}(\mathbf{g}_1^{\mathrm{d}\,H})\mathbf{H}_1^{\mathrm{d}}\mathbf{w}_1^{\mathrm{d}}))}. \tag{4.19}$$

Thus, the phase shift of $n^{th}$ element of RIS-1 is given by,

$$\begin{aligned} \phi_{1,n}^* &= \theta_0 - \arg({g_{1,n}^{\mathrm{d}}}^H {\mathbf{h}_{1,n}^{\mathrm{d}}}^H \mathbf{w}_1^{\mathrm{d}}) \\ &= \theta_0 - \arg({g_{1,n}^{\mathrm{d}}}^H) - \arg({\mathbf{h}_{1,n}^{\mathrm{d}}}^H \mathbf{w}_1^{\mathrm{d}}), \end{aligned} \tag{4.20}$$

where $g_{1,n}^H$ is $n^{th}$ element of RIS-1 and $\mathbf{h}_{1,n}^H$ is $n^{th}$ row of the $\mathbf{H}_1$. Similarly, signal to interference noise ratio (SINR) of FU is expressed as,

$$\gamma^{\mathrm{FU_d}} = \frac{\left|\left(\mathbf{g}_2^{\mathrm{d}\,H}\boldsymbol{\Phi}_2^{\mathrm{d}}\mathbf{H}_2^{\mathrm{d}} + \mathbf{h}_2^{\mathrm{d}\,H}\right)\mathbf{w}_2^{\mathrm{d}}\right|^2 (1-\alpha_1)\mathrm{P}}{\left|\left(\mathbf{g}_2^{\mathrm{d}\,H}\boldsymbol{\Phi}_2^{\mathrm{d}}\mathbf{H}_2^{\mathrm{d}} + \mathbf{h}_2^{\mathrm{d}\,H}\right)\mathbf{w}_1^{\mathrm{d}}\right|^2 \alpha_1\mathrm{P} + N_0}. \tag{4.21}$$

The SINR of FU is maximized by following the similar procedure as followed with SNR optimization of NU. Therefore, the optimal solution of phase shift $\phi_{2,n}$ at RIS-2 is given by

$$\begin{aligned} \phi_{2,n}^* &= \theta_0 - \arg({g_{2,n}^{\mathrm{d}}}^H {\mathbf{h}_{2,n}^{\mathrm{d}}}^H \mathbf{w}_2^{\mathrm{d}}) \\ &= \theta_0 - \arg({g_{2,n}^{\mathrm{d}}}^H) - \arg({\mathbf{h}_{2,n}^{\mathrm{d}}}^H \mathbf{w}_2^{\mathrm{d}}), \end{aligned} \tag{4.22}$$

where $\mathbf{h}_{2,n}^{H}$ is $n^{th}$ row of the $\mathbf{H}_2$.

### 4.2.4 Centralised Deployment of RIS-assisted NOMA System

The proposed centralized deployment of the RIS-assisted NOMA system (CDR-NOMA) is shown in Figure 4.1 [b]. In the CDR-NOMA, a single RIS is deployed near to the BS, which consists of $N = N_1 + N_2$ passive reflecting elements. The channel $\mathbf{H}^{\mathrm{c}}$ between BS to RIS follows a Rician distribution, which given as

$$\mathbf{H}^{\mathrm{c}} = \frac{1}{\sqrt{d_{\mathrm{BR}}^{\beta}}} \left( \sqrt{\frac{\mathrm{K}^{\mathrm{c}}}{\mathrm{K}^{\mathrm{c}}+1}} \tilde{\mathbf{H}}^{\mathrm{c}} + \sqrt{\frac{1}{\mathrm{K}^{\mathrm{c}}+1}} \bar{\mathbf{H}}^{\mathrm{c}} \right) \in {}^{N \times N_t}, \tag{4.23}$$

where $d_{\mathrm{BR}}$ denotes the distance between the BS and RIS. The channel between RIS to $\mathcal{U}_1$ and RIS and $\mathcal{U}_2$ are $\mathbf{g}_1^{\mathrm{c}}$ and $\mathbf{g}_2^{\mathrm{c}}$ are Rician distributed which are given as,

$$\mathbf{g}_1^{\mathrm{c}} = \frac{1}{\sqrt{d_{\mathrm{RU_1}}^{\beta}}} \sqrt{\frac{\mathrm{K}_{11}^{\mathrm{c}}}{\mathrm{K}_{11}^{\mathrm{c}}+1}} \tilde{\mathbf{g}}_1^{\mathrm{c}} + \sqrt{\frac{1}{\mathrm{K}_{11}^{\mathrm{c}}+1}} \bar{\mathbf{g}}_1^{\mathrm{c}} \in {}^{N \times 1}, \tag{4.24}$$

and

$$\mathbf{g}_2^{\mathrm{c}} = \frac{1}{\sqrt{d_{\mathrm{RU_2}}^{\beta}}} \sqrt{\frac{\mathrm{K}_{22}^{\mathrm{c}}}{\mathrm{K}_{22}^{\mathrm{c}}+1}} \tilde{\mathbf{g}}_2^{\mathrm{c}} + \sqrt{\frac{1}{\mathrm{K}_{22}^{\mathrm{c}}+1}} \bar{\mathbf{g}}_2^{\mathrm{c}} \in {}^{N \times 1}, \tag{4.25}$$

where, $\tilde{\mathbf{H}}^{\mathrm{c}}$, $\tilde{\mathbf{g}}_1^{\mathrm{c}}$ and $\tilde{\mathbf{g}}_2^{\mathrm{c}}$ are the LoS, $\bar{\mathbf{H}}^{\mathrm{c}}$, $\bar{\mathbf{g}}_1^{\mathrm{c}}$ and $\bar{\mathbf{g}}_2^{\mathrm{c}}$ are NLoS components with Rayleigh flat fading. The $\mathrm{K}^{\mathrm{c}}$, $\mathrm{K}_{11}^{\mathrm{c}}$ and $\mathrm{K}_{11}^{\mathrm{c}}$ are Rician factors. The $d_{\mathrm{RU_1}}$ and $d_{\mathrm{RU_2}}$ denote the distance between RIS to $\mathcal{U}_1$ and $\mathcal{U}_2$, respectively.

In the CDR-NOMA system, a direct link between the BS to users $\mathcal{U}_1$ and $\mathcal{U}_2$ are denoted by $\mathbf{h}_1^{\mathrm{c}}$ and $\mathbf{h}_2^{\mathrm{c}}$, respectively. These channels are considered as Rayleigh-flat fading which are independent and identical distributed (iid) with $\mathbf{h}_{\mathrm{v}}^{\mathrm{c}} \sim \mathcal{CN}(0, \sigma_v^2)$,

$v = 1, 2$. The received signals at the user $\mathcal{U}_1$ is expressed as,

$$y_1^{\mathrm{c}} = \mathbf{f}_1^{\mathrm{c}} \left( \mathbf{w}_1^{\mathrm{c}} \sqrt{\alpha_1 \mathrm{P}} x_1 + \mathbf{w}_2^{\mathrm{c}} \sqrt{(1-\alpha_1)\mathrm{P}} x_2 \right) + n_1^{\mathrm{c}}, \tag{4.26}$$

where, $\mathbf{f}_1^{\mathrm{c}} = \left( \mathbf{g}_1^{\mathrm{c}H} \mathbf{\Phi}_1^{\mathrm{c}} \mathbf{H}_1^{\mathrm{c}} + \mathbf{h}_1^{\mathrm{c}H} \right)$ denotes the direct and indirect channels for the $\mathcal{U}_1$, where $\mathbf{\Phi}_1^{\mathrm{c}} \in \mathbb{C}^{N \times N}$ is a diagonal matrix and $\mathbf{w}_1^{\mathrm{c}}$ and $\mathbf{w}_2^{\mathrm{c}}$ are a zero-forcing precoder which are given as,

$$\mathbf{w}_1^{\mathrm{c}} = \frac{\mathbf{f}_1^{\mathrm{c}H} (\mathbf{f}_1^{\mathrm{c}} \mathbf{f}_1^{\mathrm{c}H})^{-1}}{\left\| \mathbf{f}_1^{\mathrm{c}} (\mathbf{f}_1^{\mathrm{c}} \mathbf{f}_1^{\mathrm{c}H})^{-1} \right\|_2^2} \in \mathbb{C}^{N_{\mathrm{t}} \times 1}, \tag{4.27}$$

and

$$\mathbf{w}_2^{\mathrm{c}} = \frac{\mathbf{f}_2^{\mathrm{c}H} (\mathbf{f}_2^{\mathrm{c}} \mathbf{f}_2^{\mathrm{c}H})^{-1}}{\left\| \mathbf{f}_2^{\mathrm{c}} (\mathbf{f}_2^{\mathrm{c}} \mathbf{f}_2^{\mathrm{c}H})^{-1} \right\|_2^2} \in \mathbb{C}^{N_{\mathrm{t}} \times 1}. \tag{4.28}$$

Similarly, the received signals at the user $\mathcal{U}_2$ is given as,

$$y_2^{\mathrm{c}} = \mathbf{f}_2^{\mathrm{c}} \left( \mathbf{w}_1^{\mathrm{c}} \sqrt{\alpha_1 \mathrm{P}} x_1 + \mathbf{w}_2^{\mathrm{c}} \sqrt{(1-\alpha_1)\mathrm{P}} x_2 \right) + n_2^{\mathrm{c}}, \tag{4.29}$$

where, $\mathbf{f}_2^{\mathrm{c}} = \left( \mathbf{g}_2^{\mathrm{c}H} \mathbf{\Phi}^{\mathrm{c}} \mathbf{H}_2^{\mathrm{c}} + \mathbf{h}_2^{\mathrm{c}H} \right)$, and $n_v^{\mathrm{c}}, v = 1, 2$ denotes the noise. The NU and FU symbols are decoded by using SIC and ML detector respectively. The SNR and SINR are maximization of NU and FU is converted into convex semidefinite relaxation (SDR) and solved by using Gaussian randomization techniques to generate sub-optimal solutions.

### 4.2.5 SNR Optimization through Centralised Algorithm

The SNR of NU after perfect SIC is expressed as,

$$\gamma^{\mathrm{NU_c}} = \frac{\left| \left( \mathbf{g}_1^{\mathrm{c}H} \mathbf{\Phi}^{\mathrm{c}} \mathbf{H}^{\mathrm{c}} + \mathbf{h}_1^{\mathrm{c}H} \right) \mathbf{w}_1^{\mathrm{c}} \right|^2 \alpha_1 \mathrm{P}}{N_0}. \tag{4.30}$$

Similarly, the SINR of the FU is written as

$$\gamma^{\mathrm{FU_c}} = \frac{\left|\left(\mathbf{g}_2^{\mathrm{c}H}\mathbf{\Phi}^{\mathrm{c}}\mathbf{H}^{\mathrm{c}} + \mathbf{h}_2^{\mathrm{c}H}\right)\mathbf{w}_2^{\mathrm{c}}\right|^2 (1-\alpha_1)\mathrm{P}}{\left|\left(\mathbf{g}_2^{\mathrm{c}H}\mathbf{\Phi}^{\mathrm{c}}\mathbf{H}^{\mathrm{c}} + \mathbf{h}_2^{\mathrm{c}H}\right)\mathbf{w}_1^{\mathrm{c}}\right|^2 \alpha_1\mathrm{P} + N_0}. \tag{4.31}$$

The BER and sum-rate performance of CDR-NOMA depends on the maximum received SNR ($\gamma_{\max}^{\mathrm{NU_c}}$) and SINR ($\gamma_{\max}^{\mathrm{FU_c}}$) of NU and FU, which can be optimized using the phase shift $\mathbf{\Phi}$ of RIS. Let, $\mathrm{b}_{2,1} = \mathbf{h}_2^{\mathrm{c}H}\mathbf{w}_1^{\mathrm{c}}$, $\mathrm{b}_{1,1} = \mathbf{h}_1^{\mathrm{c}H}\mathbf{w}_1^{\mathrm{c}}$, $\mathbf{g}_2^{\mathrm{c}H}\mathbf{\Phi}^{\mathrm{c}}\mathbf{H}^{\mathrm{c}}\mathbf{w}_2^{\mathrm{c}} = \mathbf{u}^H\mathbf{a}_{2,2}$, and $\mathbf{g}_2^{\mathrm{c}H}\mathbf{\Phi}^{\mathrm{c}}\mathbf{H}^{\mathrm{c}}\mathbf{w}_2^{\mathrm{c}} = \mathbf{u}^H\mathbf{a}_{2,1}$, where $\mathbf{u} = [\mathrm{e}^{\phi_1}, \ldots, \mathrm{e}^{\phi_N}]^H$ and $u_n = \mathrm{e}^{\phi_n}$.

$$\begin{aligned} &\text{Find } \boldsymbol{u} \\ &\text{s.t. } \frac{|\boldsymbol{u}^H\boldsymbol{a}_{1,1} + b_{1,1}|^2}{N_0} \geq \gamma_{\max}^{\mathrm{NU_c}}, \\ &\text{s.t. } \frac{|\boldsymbol{u}^H\boldsymbol{a}_{2,2} + b_{2,2}|^2}{|\boldsymbol{u}^H\boldsymbol{a}_{2,1} + b_{2,1}|^2 + N_0} \geq \gamma_{\max}^{\mathrm{FU_c}}, \\ &|u_n| = 1, \quad n = 1, \cdots, N. \end{aligned} \tag{4.32}$$

The above constraints are non-convex and the optimization problem can be converted into quadratic constraints and then apply the SDR for sub optimal solution of (4.32) as

$$\begin{aligned} &\text{Find } \boldsymbol{u} \\ &\text{s.t. } \bar{\boldsymbol{u}}^H\boldsymbol{R}_{1,1}\bar{\boldsymbol{u}} + |b_{1,1}|^2 \geq \gamma_{\max}^{\mathrm{NU_c}} N_0 \\ &\text{s.t. } \bar{\boldsymbol{u}}^H\boldsymbol{R}_{2,2}\bar{\boldsymbol{u}} + |b_{2,2}|^2 \geq \gamma_{\max}^{\mathrm{FU_c}}\bar{\boldsymbol{u}}^H\boldsymbol{R}_{2,1}\bar{\boldsymbol{u}} \\ &\qquad + \gamma_{\max}^{\mathrm{FU}}\left(|b_{2,1}|^2 + N_0\right), \\ &|u_n|^2 = 1, \quad n = 1, \cdots, N+1, \end{aligned} \tag{4.33}$$

where

$$\boldsymbol{R}_{2,1} = \begin{bmatrix} \boldsymbol{a}_{2,1}\boldsymbol{a}_{2,1}^H & \boldsymbol{a}_{2,1}b_{2,1}^H \\ \boldsymbol{a}_{2,1}^H b_{2,1} & 0 \end{bmatrix}, \quad \bar{\boldsymbol{u}} = \begin{bmatrix} \boldsymbol{u} \\ 1 \end{bmatrix}.$$

Further, the above problem can be reduced to $\bar{\boldsymbol{u}}^H \boldsymbol{R}_{2,1} \bar{\boldsymbol{u}} = tr(\boldsymbol{R}_{2,1}) \bar{\boldsymbol{u}} \bar{\boldsymbol{u}}^H$ , with $\boldsymbol{U} = \bar{\boldsymbol{u}} \bar{\boldsymbol{u}}^H$, which satisfies $\boldsymbol{U} \geq 0$ and the rank $(\boldsymbol{U}) = 1$. Due to rank-one constraint, it is non-convex. Therefore, the above problem can be reduced to

$$
\begin{aligned}
(\text{P4}): \ & \text{Find } \boldsymbol{U} \\
& \text{s.t. } \mathrm{tr}(\boldsymbol{R}_{1,1}\boldsymbol{U}) + |b_{1,1}|^2 \geq \gamma_{\max}^{\mathrm{NU_c}} \\
& \text{s.t. } \mathrm{tr}(\boldsymbol{R}_{2,2}\boldsymbol{U}) + |b_{2,2}|^2 \geq \gamma_{\max}^{\mathrm{FU_c}} \mathrm{tr}(\boldsymbol{R}_{2,1}\boldsymbol{U}) \\
& \quad \boldsymbol{U}_{n,n} = 1, n = 1, \cdots, N+1, \\
& \quad \boldsymbol{U} \succeq 0.
\end{aligned} \tag{4.34}
$$

where

$$
\boldsymbol{R}_{1,1} = \begin{bmatrix} \boldsymbol{a}_{1,1}\boldsymbol{a}_{1,1}^H & \boldsymbol{a}_{2,1} b_{1,1}^H \\ \boldsymbol{a}_{1,1}^H b_{1,1} & 0 \end{bmatrix}, \quad \boldsymbol{R}_{2,2} = \begin{bmatrix} \boldsymbol{a}_{2,2}\boldsymbol{a}_{2,2}^H & \boldsymbol{a}_{2,1} b_{2,2}^H \\ \boldsymbol{a}_{2,2}^H b_{2,2} & 0 \end{bmatrix}.
$$

The above problem (P4) is a convex SDR, which doesn't satisfy the rank $(\mathbf{U}) = 1$. Therefore, to obtain rank one solution, we have implemented Gaussian randomization technique and eigenvalue decomposition of $\mathbf{U}$ as $\mathbf{U} = \mathbf{V}\Sigma\mathbf{V}^H$. where $\mathbf{V} \in \mathbb{C}^{(N+1)\times(N+1)}$ and $\Sigma^{\frac{1}{2}} \triangleq \mathrm{diag}\{\sqrt{\xi_1}, \ldots, \sqrt{\xi_{N+1}}\}$. A sub-optimal solution of (P4) is

$$
\tilde{\mathbf{u}} = \mathbf{V}\Sigma^{\frac{1}{2}}\mathbf{r}, \tag{4.35}
$$

where, $\mathbf{r} \sim \mathcal{CN}(0, \mathbf{I}_{N+1})$ is random vector. Further, we generate a sub-optimal solution of $\mathbf{U}$ is given as, $\hat{\mathbf{u}} = \mathrm{e}^{j\angle([\frac{\tilde{\mathbf{u}}}{\tilde{\mathbf{u}}_{N+1}}]_{(1:N)})}$.

### 4.2.6 Sum-Rate Analysis

The total sum-rate $\mathcal{R}^{\mathrm{d}}$ of DDR-NOMA system is expressed as,

$$\mathcal{R}^{\mathrm{d}} = \mathcal{R}^{\mathrm{NU_d}} + \mathcal{R}^{\mathrm{FU_d}} \tag{4.36}$$

where $\mathcal{R}^{\mathrm{NU_d}}$ and $\mathcal{R}^{\mathrm{FU_d}}$ are the sum-rate of NU and FU, respectively, which are given as,

$$\mathcal{R}^{\mathrm{NU_d}} = \log_2\left(1+\gamma^{\mathrm{NU_d}}\right), \text{ and}$$

$$\mathcal{R}^{\mathrm{FU_d}} = \log_2\left(1+\gamma^{\mathrm{FU_d}}\right). \tag{4.37}$$

Similarly, the total sum-rate $\mathcal{R}^{\mathrm{c}}$ of CDR-NOMA system respectively, which are given as,

$$\mathcal{R}^{\mathrm{c}} = \mathcal{R}^{\mathrm{NU_c}} + \mathcal{R}^{\mathrm{FU_c}} \tag{4.38}$$

where, $\mathcal{R}^{\mathrm{NU_c}}$ and $\mathcal{R}^{\mathrm{FU_c}}$ are sum-rate of NU and FU in CDR-NOMA system as,

$$\mathcal{R}^{\mathrm{NU_c}} = \log_2\left(1+\gamma^{\mathrm{NU_c}}\right), \text{ and}$$

$$\mathcal{R}^{\mathrm{FU_c}} = \log_2\left(1+\gamma^{\mathrm{FU_c}}\right), \tag{4.39}$$

where $\gamma^{\mathrm{NU_c}}$ and $\gamma^{\mathrm{FU_c}}$ denote the SNR of NU and FU, respectively in CDR-NOMA. Moreover, the maximum sum-rate of the proposed system is achievable by maximizing the SNR and SINR of NU and FU in CDR-NOMA and DDR-NOMA system.

## 4.3 Simulation Results and Discussions

The locations of BS, NU and FU's are chosen as (0,0,10) m, (200,0,1) m, and $(-400,0,1)$m respectively. In DDR-NOMA system, two RISs are located at (200,0,2)

m and (−400,0,2) m, where in the CDR-NOMA system, single RIS is deployed at (0,0,9) m. Therefore, the distance between the RIS and BS in the CDR-NOMA system is equal to the corresponding distances of RISs to users in the DDR-NOMA system [94]. The power coefficients of NU and FU are 0.4 and 0.6, respectively. The noise power spectral density and bandwidth is set as is −173 dBm/Hz, and $BW = 180$ kHz, with Rician fading respectively. Further, path loss exponents through RIS and direct paths are $\beta = 3$ and $\eta = 3.5$, respectively. However, the reference channel power gain is −30 dB at a distance of 1 m, and reflecting elements are chosen as $N = 32$, $N_1 = 16$, and $N_2 = 16$.

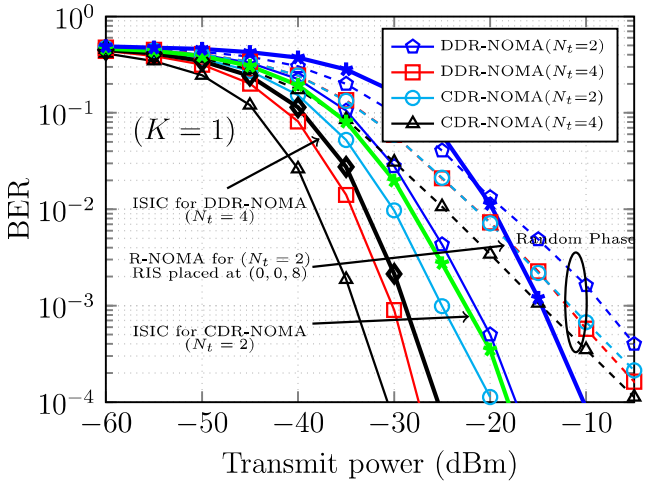


FIGURE 4.2: Average BER performance of NU in DDR-NOMA and CDR-NOMA system for $N_t = 2, 4$. The solid lines denote optimized $\mathbf{\Phi}$ through SDR and dashed lines denote the random phase.

The BER performance of the NU and FU is shown in Figure 4.2 and Figure 4.3, respectively for the proposed CDR-NOMA and DDR-NOMA. In the proposed system, BER performance is improved as the number of increasing transmit antennas $N_{\mathrm{t}}$ increases along with beamforming at transmitter, as observed in Figure 4.2 and Figure 4.3. A virtual MIMO system is established between BS and RIS in a RIS-assisted NOMA. Further, the BER performance of CDR-NOMA is better than the

DDR-NOMA due to enhanced passive beamforming gain. Furthermore, BER performance of both NU and FU also depends on phase of RIS $\mathbf{\Phi}$, as shown in results. The phase matrix is optimized through the SDR and it gives the diversity gain as compared to random phase of RIS, as shown in Figure 4.2 and Figure 4.3.

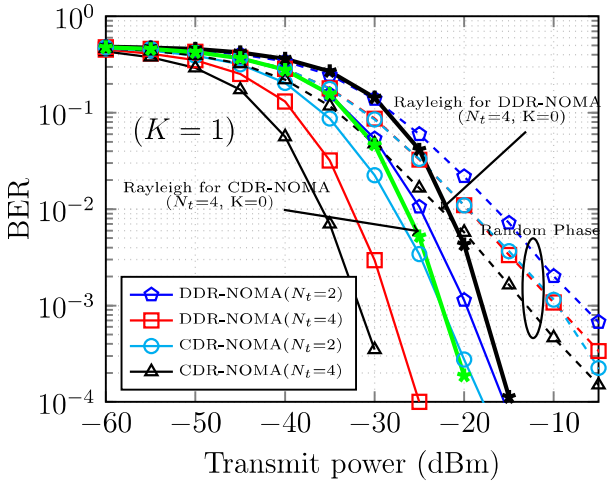


FIGURE 4.3: Average BER performance of FU in DDR-NOMA and CDR-NOMA system for $N_t = 2, 4$. The solid lines denote optimized $\mathbf{\Phi}$ through SDR and dashed lines denote the random phase.

From Figure 4.2 and Figure 4.3, it is observed that the BER performance of NU is better than the FU. Since perfect SIC at NU mitigates the interference of FU signal. Further imperfect SIC (ISIC) is applied to the DDR-NOMA and CDR-NOMA for $N_{\mathrm{t}} = 2$ and $N_{\mathrm{t}} = 4$ and it is observed that ISIC degrades BER, as shown in Figure 4.2 because ISIC reduces the maximized received signal strength[1]. Further, impact of Rician factor $K$ is also considered in Figure 4.3, and observe that the Ricean fading $(K = 1)$ has better performance than Rayleigh fading $(K = 0)$ channel. Figure 4.3 also highlights that the proposed RIS-assisted NOMA system performance is better than the conventional RIS assisted NOMA (R-NOMA) [69].

[1]SNR in ISIC is $\frac{\left|\left(\mathbf{g}_1^{\mathrm{d}H}\mathbf{\Phi}_1^{\mathrm{d}}\mathbf{H}_1^{\mathrm{d}}+\mathbf{h}_1^{\mathrm{d}H}\right)\mathbf{w}_1^{\mathrm{d}}\right|^2\alpha_1\mathrm{P}}{\left|\left(\mathbf{g}_1^{\mathrm{d}H}\mathbf{\Phi}_1^{\mathrm{d}}\mathbf{H}_1^{\mathrm{d}}+\mathbf{h}_1^{\mathrm{d}H}\right)\mathbf{w}_1^{\mathrm{d}}\right|^2\kappa\alpha_2\mathrm{P}+N_0}$ [79], where $\kappa \neq 0$ denotes the ISIC parameter. In case of perfect SIC $\kappa = 0$.

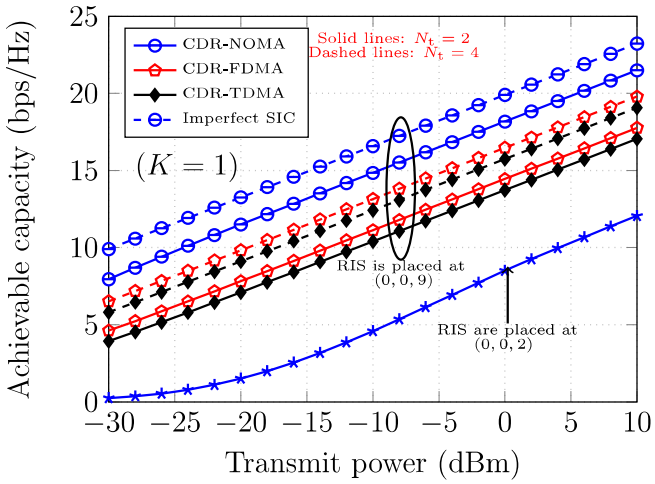


FIGURE 4.4: Sum-rate performance of CDR-NOMA, and TDMA and FDMA-based OMA systems for $N_t = 2, 4$.

Next, Figure 4.4 and Figure 4.5 show the sum-rate performance of the proposed centralised and distributed RIS-assisted NOMA system, respectively, with TDMA and FDMA OMA systems. The proposed CDR-NOMA and DDR-NOMA achieve better sum-rate than FDMA and TDMA system, as shown in Figure 4.4 due to superimposition of users in the power domain and SIC-based their receiver design. In case of imperfect SIC (ISIC), the sum-rate is degraded at higher transmit power due to the presence of interference at NU, as observed in Figure 4.4 and Figure 4.5. Further, the sum-rate is enhanced as the number of transmit antennas $N_{\mathrm{t}}$ increases and improved beamforming at the BS. Furthermore, the sum-rate performance of DDR-NOMA system is inferior to CDR-NOMA system, as observed from Figure 4.4 and Figure 4.5 due to the channel beamforming gain of centralised RIS is higher than distributed RISs. Figure 4.4 and Figure 4.5, also highlight that sum-rate performance is degraded when RIS is far from the users or the BS due to reduced channel beamforming gain.

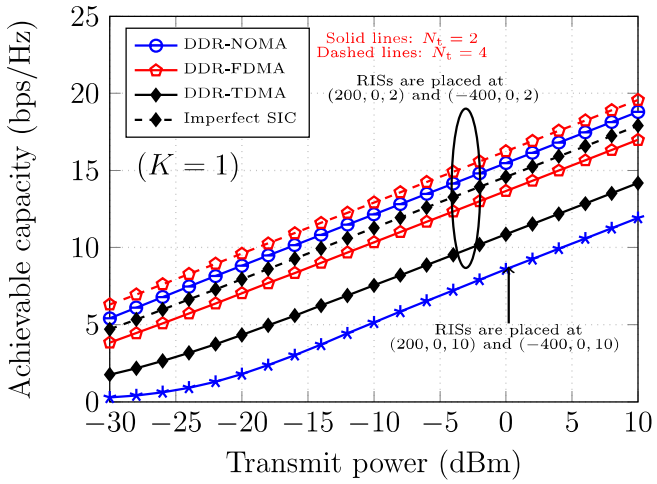


FIGURE 4.5: Sum-rate performance of DDR-NOMA, and TDMA and FDMA-based OMA systems for $N_t = 2, 4$.

## 4.4 Proposed Multiple RIS Assisted NOMA System Model

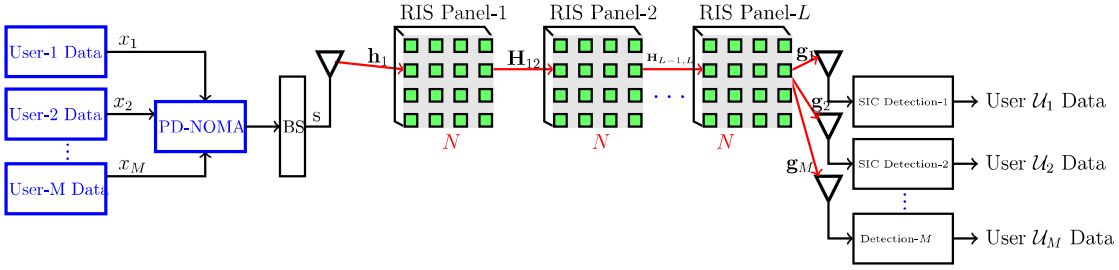


FIGURE 4.6: The proposed multiple RIS-assisted NOMA system model.

The block diagram of proposed MR-NOMA is shown in Figure4.6, in which the BS consists single transmit antenna, and it is communicating to $M$ number of NOMA users $(\mathcal{U}_1, ....\mathcal{U}_M)$ through multiple RISs and each user has a single receive antenna. Let $L$ be the number of multiple RISs with $N$ reflecting elements. MRISs create a virtual LoS channel between BS and $M$ users. The users $\mathcal{U}_1$ and $\mathcal{U}_M$ are the nearest user (NU) and farthest user (FU) from the last RIS panel ($L$), respectively.

Therefore, the channel gains of users are represented as $||\mathbf{g}_{L1}|| > ||\mathbf{g}_{L2}|| \cdots > ||\mathbf{g}_{LM}||$, and their corresponding distances from the last RIS panel $L$ are $d_{LM} > \cdots d_{L2} > d_{L1}$. The power coefficients $\alpha_M > \cdots \alpha_2 > \alpha_1$ are assigned to the farthest to nearest users, respectively, based on their channel gains.

The channel between the BS and the first RIS is $\mathbf{h}_1 \in \mathbb{C}^{1\times N}$, and it follows a Rician distribution, which is given as

$$\mathbf{h}_1 = \frac{1}{\sqrt{d_{\mathrm{BR}}^{\beta}}}\left(\sqrt{\frac{\mathrm{K}_1}{\mathrm{K}_1+1}}\tilde{\mathbf{h}}_1 + \sqrt{\frac{1}{\mathrm{K}_1+1}}\bar{\mathbf{h}}_1\right) \in \mathbb{C}^{1\times N}, \tag{4.40}$$

where, $d_{\mathrm{BR}}$ is the distance between the BS and the first RIS, and $\beta \geq 2$ represents the path loss exponent [55]. The $\tilde{\mathbf{h}}_1$ and $\bar{\mathbf{h}}_1$ represent the LoS and non-LoS (NLoS) components with Rayleigh flat fading and $\mathrm{K}_1$ denotes the Rician factor. Similarly, the channel vector $\mathbf{g}_{Lm} \in \mathbb{C}^{N\times 1}$ between the last RIS-L and the $m$-th user ($m = 1, \cdots, M$) is Rician distributed which is given as

$$\mathbf{g}_{Lm} = \frac{1}{\sqrt{d_{Lm}^{\beta}}}\sqrt{\frac{\mathrm{K}_{Lm}}{\mathrm{K}_{Lm}+1}}\tilde{\mathbf{g}}_{Lm} + \sqrt{\frac{1}{\mathrm{K}_{Lm}+1}}\bar{\mathbf{g}}_{Lm} \in \mathbb{C}^{N\times 1}, \tag{4.41}$$

where, $\tilde{\mathbf{g}}_{Lm}$ and $\bar{\mathbf{g}}_{Lm}$ are the LoS and NLoS components with Rayleigh flat fading and $\mathrm{K}_{Lm}$ is Rician factor and $d_{Lm}$ is the distance between RIS-L to the $m$-th user. Finally channel between the $l$-th RIS and the $(l+1)$-th RIS as $\mathbf{H}_{(l,l+1)} \in \mathbb{C}^{N\times N}$ is a Rician flat fading channel, which is independent and identically distributed (iid) with $\mathbf{H}_{(l,l+1)} \sim \mathcal{CN}(0,1)$. The channel $\mathbf{H}_{(l,l+1)}$ is expressed as

$$\mathbf{H}_{l,l+1} = \frac{1}{\sqrt{d_{l,l+1}^{\beta}}}\left(\sqrt{\frac{\mathrm{K}_{l,l+1}}{\mathrm{K}_{l,l+1}+1}}\tilde{\mathbf{H}}_{l,l+1} + \sqrt{\frac{1}{\mathrm{K}_{l,l+1}+1}}\bar{\mathbf{H}}_{l,l+1}\right), \tag{4.42}$$

where, $d_{l,l+1}$ is the distance between $l$-th RIS to $(l+1)$-th RIS. Moreover, the received signal at $m$-th user is given by,

$$y_m = \frac{1}{\sqrt{P_m}} \left( \mathbf{h}_1 \left( \prod_{l=1}^{L-1} \mathbf{H}_{l,l+1} \Phi_l \right) \Phi_L \mathbf{g}_{Lm} \right) \mathrm{s} + n_m, \tag{4.43}$$

where, $\mathbf{\Phi}_l$ is a diagonal matrix given as $\mathbf{\Phi}_l = \mathrm{diag}[A_{l1}\mathrm{e}^{\phi_{l1}}, A_{l2}\mathrm{e}^{\phi_{l2}}, \ldots, A_{lN}\mathrm{e}^{\phi_{lN}}]$, where $A_{ln} \in (0,1]$ denotes the amplitude reflection coefficient, in general $|A_{ln}| = 1 \ \forall n, l$ [95]. The $\phi_{ln}$ is phase shift induced by $n$-th element of the $l$-th RIS panel, and s is a superposed symbol written as

$$\mathrm{s} = \sum_{m=1}^{M} \sqrt{\mathrm{P}_t \alpha_m} x_m, \tag{4.44}$$

where $\mathrm{P}_t$ is the total transmit power available at BS and $\alpha_m$ denotes the power coefficient of $m$-th user. The $x_m$ denotes the $m$-th user's binary phase shift keying (BPSK) modulated symbol. The $n_m$ denotes additive white Gaussian noise (AWGN) with $\sim \mathcal{CN}(0, N_0)$. $P_m = d_{\mathrm{BR}}^{\beta} \left( \prod_{l=1}^{L-1} d_{l,l+1}^{\beta} \right) d_{Lm}^{\beta}$ is path loss between BS and $m$-th user.

### 4.4.1 Detection of NOMA Users

In the MR-NOMA, $M$ users are multiplexed in the power domain and a higher power level is assigned to $\mathcal{U}_M$ user as it is being far from the BS. the user $\mathcal{U}_M$ is detected directly from the received signal by using the maximum likelihood (ML) detector. The remaining $(M-1)$ users apply first SIC to remove substantial far user interference, ML detector is used decode own symbols. The far user $\mathcal{U}_M$ received

signal is given as,

$$y_M^{\mathrm{FU}} = \frac{1}{\sqrt{P_M}} \left( \mathbf{h}_1 \left( \prod_{l=1}^{L-1} \mathbf{H}_{l,l+1} \Phi_l \right) \Phi_L \mathbf{g}_{LM} \right) \mathrm{s} + n_M. \tag{4.45}$$

Therefore, user $\mathcal{U}_M$'s data is decoded using ML detector which is given by

$$\hat{x}_M^{\mathrm{FU}} = \arg \min_{x_M \in \mathcal{X}_M} \left\| y_M^{\mathrm{FU}} - \frac{1}{\sqrt{P_M}} \left( \mathbf{h}_1 \left( \prod_{l=1}^{L-1} \mathbf{H}_{l,l+1} \Phi_l \right) \Phi_L \mathbf{g}_{LM} \right) \mathrm{s} \right\|_2^2. \tag{4.46}$$

The remaining $(M-1)$ users are near to BS, and first using SIC interference of FU users' is removed from the received signal, $m$-th user extracts information by applying ML detection. Therefore $m$-th user signal after SIC is expressed as

$$y_{m,\mathrm{SIC}}^{\mathrm{NU}} = \left\{ y_m^{\mathrm{NU}} - \left[ \frac{1}{\sqrt{P_m}} \left( \mathbf{h}_1 \left( \prod_{l=1}^{L-1} \mathbf{H}_{l,l+1} \Phi_l \right) \Phi_L \mathbf{g}_{Lm} \right) \hat{x}_{m+1} \right] \right\}, \tag{4.47}$$

where, $y_m^{\mathrm{NU}}$ is the $m$-th user received signal as defined in (4.43), and $\hat{x}_{m+1}$ is interference signal decoded at $m$-th user. Further, $m$-th user information extracts from $y_{m,\mathrm{SIC}}^{\mathrm{NU}}$ by using ML detector as

$$\hat{x}_m^{\mathrm{NU}} = \arg \min_{x_m \in \mathcal{X}_m} \left\| y_{m,\mathrm{SIC}}^{\mathrm{NU}} - \frac{1}{\sqrt{P_m}} \left( \mathbf{h}_1 \left( \prod_{l=1}^{L-1} \mathbf{H}_{l,l+1} \Phi_l \right) \Phi_L \mathbf{g}_{Lm} \right) \mathrm{s} \right\|_2^2. \tag{4.48}$$

## 4.5 Performance Analysis of MR-NOMA users

In this section, BEP of MR-NOMA users is analyzed. In the present analysis, the BS transmits superimposed symbols of two users through three multiple RISs ($L = 3$). The user $\mathcal{U}_1$ and $\mathcal{U}_2$ are near and far from the RIS-3, respectively. Further, the

received signal of far user $\mathcal{U}_2$ is expressed as,

$$y_2 = \frac{1}{\sqrt{P_2}} \left( \mathbf{h}_1 \left( \prod_{l=1,2} \mathbf{H}_{l,l+1} \mathbf{\Phi}_l \right) \mathbf{\Phi}_3 \mathbf{g}_{32} \right) \mathrm{s} + n_2, \tag{4.49}$$

where $P_2 = d_{\mathrm{BR}}^{\beta} d_{1,2}^{\beta} d_{2,3}^{\beta} d_{32}^{\beta}$ is the path loss component from the BS to FU.

The FU's information is decoded using ML detector which is given as,

$$\hat{x}_2 = \arg \min_{x_2 \in \mathcal{X}_2} \left\| y_2 - \frac{1}{\sqrt{P_2}} \left( \mathbf{h}_1 \left( \prod_{l=1,2} \mathbf{H}_{l,l+1} \mathbf{\Phi}_l \right) \mathbf{\Phi}_3 \mathbf{g}_{32} \right) \mathrm{s} \right\|_2^2. \tag{4.50}$$

Moreover, the received signal at the NU is represented as,

$$y_1 = \frac{1}{\sqrt{P_1}} \left( \mathbf{h}_1 \left( \prod_{l=1,2} \mathbf{H}_{l,l+1} \mathbf{\Phi}_l \right) \mathbf{\Phi}_3 \mathbf{g}_{31} \right) \mathrm{s} + n_1, \tag{4.51}$$

where, $P_1 = d_{\mathrm{BR}}^{\beta} d_{1,2}^{\beta} d_{2,3}^{\beta} d_{31}^{\beta}$ is the path loss component from BS to NU. The NU information is decoded by using SIC, therefore first remove FU interference from the $y_1$, after that ML detector is used. The FU data is extracted by the ML detector at NU as,

$$\hat{x}_2^{NU} = \arg \min_{x_2 \in \mathcal{X}_2} \left\| y_1 - \frac{1}{\sqrt{P_1}} \left( \mathbf{h}_1 \left( \prod_{l=1,2} \mathbf{H}_{l,l+1} \mathbf{\Phi}_l \right) \mathbf{\Phi}_3 \mathbf{g}_{31} \right) \mathrm{s} \right\|_2^2. \tag{4.52}$$

The extracted information, $\hat{x}_2^{\mathrm{NU}}$ is subtracted from the received signals $y_1$ as,

$$y_1^{\mathrm{SIC}} = y_1 - \left[ \frac{1}{\sqrt{P_1}} \left( \mathbf{h}_1 \left( \prod_{l=1,2} \mathbf{H}_{l,l+1} \mathbf{\Phi}_l \right) \mathbf{\Phi}_3 \mathbf{g}_{31} \right) \hat{x}_2^{\mathrm{NU}} \right]. \tag{4.53}$$

A NU symbol is decoded from $y_1^{\mathrm{SIC}}$ by using ML decoder as,

$$\hat{x}_1 = \arg \min_{x_1 \in \mathcal{X}_1} \left\| y_1^{\mathrm{SIC}} - \frac{1}{\sqrt{P_1}} \left( \mathbf{h}_1 \left( \prod_{l=1,2} \mathbf{H}_{l,l+1} \mathbf{\Phi}_l \right) \mathbf{\Phi}_3 \mathbf{g}_{31} \right) \mathrm{s} \right\|_2^2. \tag{4.54}$$

The channels fading coefficients among RIS-1 to RIS-2 and RIS-2 to RIS-3 are expressed as $\mathbf{H}_{12} = \mu_{ij}\mathrm{e}^{-j\psi_{ij}}$ and $\mathbf{H}_{23} = \lambda_{jk}\mathrm{e}^{-j\psi_{jk}}$ respectively. The LoS channels are created among RISs as $i$-th element of RIS-1 to $j$-th element of RIS-2 and $j$-th element of RIS-2 to $k$-th element of RIS-3 with $i, j,\ k \in \mathcal{N}, (\mathcal{N} = 1, 2, \ldots, N)$. The channel fading coefficients from RIS-3 to NU and FU are $\mathbf{g}_{31} = \zeta_k^{\mathrm{NU}}\mathrm{e}^{-j\varphi_k^{\mathrm{NU}}}$ and $\mathbf{g}_{32} = \zeta_k^{\mathrm{FU}}\mathrm{e}^{-j\varphi_k^{\mathrm{FU}}}$ respectively. Further, channel fading coefficient from BS to RIS-1 is $\mathbf{h}_1 = \xi_i\mathrm{e}^{-j\nu_i}$. The SNR of FU is expressed as

$$\gamma^{\mathrm{FU}} = \frac{\left|\left(\sum_{i=1}^{N}\sum_{j=1}^{N}\sum_{k=1}^{N}\xi_i\mu_{ij}\lambda_{jk}\zeta_k^{\mathrm{FU}}\mathrm{e}^{\Delta\phi}\right)\right|^2\alpha_2\mathrm{P}_t}{\alpha_1\mathrm{P}_t + P_2N_0}, \tag{4.55}$$

where, $\Delta\phi = (\theta - \nu_i - \psi_{ij} - \psi_{jk} - \varphi_k^{\mathrm{FU}})$. The maximized SNR at FU by adjusting phase, $\Delta\phi = 0$, which is obtained as

$$\begin{aligned}\gamma_{\max}^{\mathrm{FU}} =& \frac{\left|\left(\sum_{i=1}^{N}\sum_{j=1}^{N}\sum_{k=1}^{N}\xi_i\mu_{ij}\lambda_{jk}\zeta_k^{\mathrm{FU}}\right)\right|^2\alpha_2\mathrm{P}_t}{\alpha_1\mathrm{P}_t + P_2N_0} \\ =& \frac{Z_{\mathrm{FU}}\alpha_2\mathrm{P}_t}{\alpha_1\mathrm{P}_t + P_2N_0},\end{aligned} \tag{4.56}$$

where

$$Z_{\mathrm{FU}} = \left|\left(\sum_{i=1}^{N}\sum_{j=1}^{N}\sum_{k=1}^{N}\xi_i\mu_{ij}\lambda_{jk}\zeta_k^{\mathrm{FU}}\right)\right|^2. \tag{4.57}$$

All channel coefficients are identically independent and follow Rician distribution, where $Z_{\mathrm{FU}}$ follows Gaussian distribution with mean and variance which are expressed as [76]

$$E\{Z_{\mathrm{FU}}\} = N^3\sqrt{\frac{\pi^4}{64P_2(K+1)^4}}L_{\frac{1}{2}}^4(-K^2/K+1)),$$

and

$$\mathrm{VAR}\{Z_{\mathrm{FU}}\} = \frac{N^3}{P_2}\left(1 - \frac{\pi^4}{64(K+1)^4}L_{\frac{1}{2}}^8(-K^2/K+1)\right), \tag{4.58}$$

where $L_{\frac{1}{2}}(.)$ denotes the Laguerre polynomial of degree 1/2 and $K$ is the Rician

factor [2]. The maximized SNR of FU ($\gamma_{\max}^{\mathrm{FU}}$) is obtained by applying non-central chi-square distribution with a degree of freedom is one. Therefore, its moment generating function (MGF) is expressed as,

$$M_{\gamma_{\max}^{\mathrm{FU}}}(s) = \frac{\exp\left(\frac{\frac{sN^6\pi^4 L_{1/2}^8\left(-K^2/K+1\right)\alpha_2 \mathrm{P}_t}{64(K+1)^4(\alpha_1 \mathrm{P}_t + P_2 N_0)}}{1-\frac{sN^3\left[64(K+1)^4-\pi^4 L_{1/2}^8(-K^2/K+1)\right]\alpha_2 P_t}{32(K+1)^4(\alpha_1 \mathrm{P}_t + P_2 N_0)}}\right)}{\sqrt{1-\frac{sN^3\left[64(K+1)^4-\pi^2 L_{1/2}^8(-K^2/K+1)\right]\alpha_2 \mathrm{P}_t}{32(K+1)^4(\alpha_1 \mathrm{P}_t + P_2 N_0)}}}. \tag{4.59}$$

Furthermore, in general, the BEP for BPSK can be expressed as,

$$P_e = \frac{1}{\pi}\int_0^{\pi/2} M_{\gamma_{\max}}\left(-\frac{1}{\sin^2\eta}\right) d\eta. \tag{4.60}$$

Therefore, the average BEP (ABEP) for the FU of BPSK is expressed as,

$$P_e^{\mathrm{FU}} = \frac{1}{\pi}\int_0^{\pi/2} \frac{1}{\sqrt{1+\frac{N^3\left[64(K+1)^4-\pi^4 L_{1/2}^8(-K^2/K+1)\right]\alpha_2 \mathrm{P}_t}{32(K+1)^4(\alpha_1 \mathrm{P}_t + P_2 N_0)\sin^2\eta}}} \times \exp\left(-\frac{\frac{N^6\pi^4 L_{1/2}^8\left(-K^2/K+1\right)\alpha_2 \mathrm{P}_t}{64(K+1)^4(\alpha_1 \mathrm{P}_t + P_2 N_0)\sin^2\eta}}{1+\frac{N^3\left[64(K+1)^4-\pi^4 L_{1/2}^8(-K^2/K+1)\right]\alpha_2 P_t}{32(K+1)^4(\alpha_1 \mathrm{P}_t + P_2 N_0)\sin^2\eta}}\right) d\eta. \tag{4.61}$$

The upper bound of ABEP for FU at $\eta = \pi/2$ is represented as,

$$P_e^{\mathrm{FU}} \leq \frac{0.5\exp\left(\frac{-\frac{N^6\pi^4 L_{1/2}^8\left(-K^2/K+1\right)\alpha_2 \mathrm{P}_t}{64(K+1)^4(\alpha_1 \mathrm{P}_t + P_2 N_0)}}{1+\frac{N^3\left[64(K+1)^4-\pi^4 L_{1/2}^8(-K^2/K+1)\right]\alpha_2 \mathrm{P}_t}{32(K+1)^4(\alpha_1 \mathrm{P}_t + P_2 N_0)}}\right)}{\sqrt{1+\frac{N^3\left[64(K+1)^4-\pi^4 L_{1/2}^8(-K^2/K+1)\right]\alpha_2 \mathrm{P}_t}{32(K+1)^4(\alpha_1 \mathrm{P}_t + P_2 N_0)}}}. \tag{4.62}$$

[2]For simplicity, we consider $K_1 = K_{Lm} = K_{l,l+1} = K$ henceforth.

Similarly, the maximized SNR at NU is expressed as,

$$\begin{aligned}\gamma_{\max}^{\mathrm{NU}} =& \frac{\left|\left(\sum_{i=1}^{N}\sum_{j=1}^{N}\sum_{k=1}^{N}\xi_i\mu_{ij}\lambda_{jk}\zeta_k^{\mathrm{NU}}\right)\right|^2\alpha_1\mathrm{P}_t}{P_1N_0}\\ =& \frac{Z_{\mathrm{NU}}\alpha_1\mathrm{P}_t}{P_1N_0},\end{aligned} \tag{4.63}$$

where,

$$Z_{\mathrm{NU}} = \left|\left(\sum_{i=1}^{N}\sum_{j=1}^{N}\sum_{k=1}^{N}\xi_i\mu_{ij}\lambda_{jk}\zeta_k^{\mathrm{NU}}\right)\right|^2. \tag{4.64}$$

Moreover, the upper bound of ABEP for NU is expressed as,

$$P_e^{\mathrm{NU}} \leq \frac{0.5\exp\left(\frac{-\frac{N^6\pi^4L_{1/2}^8\left(-K^2/K+1\right)\alpha_1\mathrm{P}_t}{64(K+1)^4P_1N_0}}{1+\frac{N^3\left[64(K+1)^4-\pi^4L_{1/2}^8(-K^2/K+1)\right]\alpha_1\mathrm{P}_t}{32(K+1)^4P_1N_0}}\right)}{\sqrt{1+\frac{N^3\left[64(K+1)^4-\pi^4L_{1/2}^8(-K^2/K+1)\right]\alpha_1\mathrm{P}_t}{32(K+1)^4P_1N_0}}}. \tag{4.65}$$

Proof. See Appendix I.

Further, from (4.62) the approximate BEP for FU, at high SNR is expressed as,

$$P_e^{\mathrm{FU}} \propto \frac{\exp\left(-\frac{N^3\pi^4L_{1/2}^8\left(-K^2/K+1\right)}{2\left[64(K+1)^4-\pi^4L_{1/2}^8(-K^2/K+1)\right]}\right)}{\sqrt{\frac{N^3\left[64(K+1)^4-\pi^4L_{1/2}^8(-K^2/K+1)\right]\alpha_2\mathrm{P}_t}{32(K+1)^4(\alpha_1\mathrm{P}_t+P_2N_0)}}}. \tag{4.66}$$

Therefore, BEP decreases as the number of passive reflecting surfaces $N$ increases at the RIS panels.

Next, we consider $M$-ary PSK (phase shift keying) modulation scheme to highlight the impact of modulation order in MR-NOMA. The average symbol error probability

(ASEP) $P_e^{\mathrm{NU}}$ of NU for M-ary PSK is expressed as,

$$P_e^{\mathrm{NU}} = \frac{1}{\pi}\int_0^{(M-1)\pi/M} \frac{1}{\sqrt{1+\frac{N^3\sin^2(\pi/M)\left[64(K+1)^4-\pi^4 L_{1/2}^8(-K^2/K+1)\right]\alpha_1 \mathrm{P}_t}{32(K+1)^4(P_1N_0)\sin^2\eta}}} \times \exp\left(-\frac{\frac{N^6\sin^2(\pi/M)\pi^4 L_{1/2}^8\left(-K^2/K+1\right)\alpha_1 \mathrm{P}_t}{64(K+1)^4(P_1N_0)\sin^2\eta}}{1+\frac{N^3\sin^2(\pi/M)\left[64(K+1)^4-\pi^4 L_{1/2}^8(-K^2/K+1)\right]\alpha_1 P_t}{32(K+1)^4(P_1N_0)\sin^2\eta}}\right) d\eta. \tag{4.67}$$

The upper bound of ASEP is expressed $P_e^{\mathrm{NU}}$ by setting $\eta = \pi/2$ and considering only exponential term is expressed [46] as,

$$P_e^{\mathrm{NU}} \propto \exp\left(-\sin^2(\pi/M)\frac{N^6\pi^4 L_{1/2}^8\left(-K^2/K+1\right)\alpha_1 \mathrm{P}_t}{64(K+1)^4(P_1N_0)}\right). \tag{4.68}$$

Therefore, the ASEP deteriorates for higher-order modulation schemes.

## 4.6 Simulation Results and Discussions

In this section, simulation results ARE presented and also validated them with the derived BEP. In simulations, three cascaded RISs ($L = 3$) are considered between the BS and the users. Distances between RIS-3 to NU and FU are $d_{31} = 10$m and $d_{32} = 40$m, respectively in the MR-NOMA. The power coefficients $\alpha_1 = 0.3$ and $\alpha_2 = 0.7$ for NU and FU under Rician fading channel with BPSK modulation are considered. We set system bandwidth $BW = 180$ kHz, $\beta = 2$, and noise power spectral density is $-173$ dBm/Hz. The reference channel power gain set as $-30$ dB at distance $d_0 = 1$m. in the present simulation, the different positions of RIS panels from the BS as $d_{\mathrm{BR}} = 67m, d_{1,2} = 67m, d_{2,3} = 67m$ (*Case-1*) and $d_{\mathrm{BR}} = 1m, d_{1,2} = 10m, d_{2,3} = 190m$ (*Case-2*) in simulations.

Figure 4.7 and Figure 4.8 show the average the BEP performance of NU and FU,

respectively for different values of $N = 32, 64$ and 128. As $N$ increases, BEP improves since error probability $P_e^{\text{NU}} \propto e^{-N^6}$ (in (4.65)). Further, simulation results are validated with derived ABEP (22) in Figure 4.7 and Figure 4.8. Furthermore, the proposed MR-NOMA system achieves low BEP at low transmit power. Since the multiple RISs create LoS channels between BS and users, therefore fading channel is converted into more constructive channel with the help of passive beamforming. The BEP depends on the positions of the RIS panels, as observed in Figure 4.7 and Figure 4.8. In *Case-1*, RIS-1 is far from the BS, and the distance between two RISs is also high; therefore, the BEP performance in *Case-1* degrades as compared to *Case-2*, as observed in Figure 4.7 and Figure 4.8. Next, we find that FU has degrades performance as compared to NU due to the presence of interference in symbol detection (as given in (4.45)). RIS panels between BS and FU enhance the cell-edge user $\mathcal{U}_2$'s performance. Therefore, MR-NOMA system improves network coverage for a fixed transmit power, as observed in Figure 4.7 and Figure 4.8.

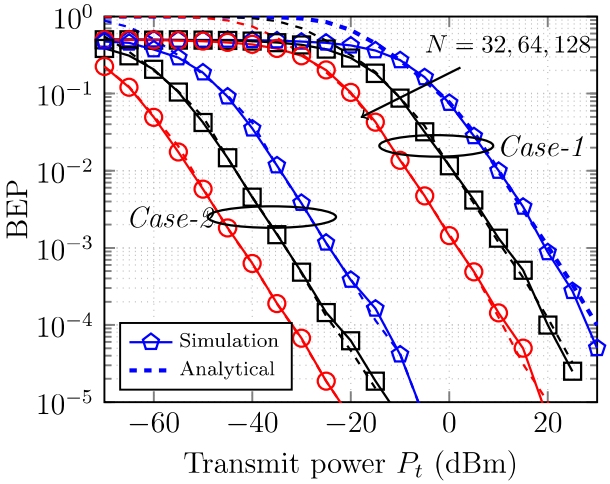


FIGURE 4.7: Average BEP performance of NU by varying reflecting elements $N$ and RISs panels positions.

Figure 4.9 shows average BEP of NU in the proposed MR-NOMA, RIS-NOMA [56], and RIS-selection based transmission over multiple RISs (RSBT) [76]. The NU's

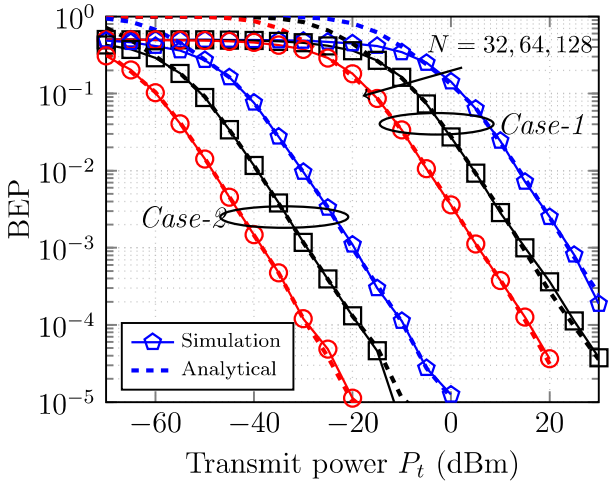


FIGURE 4.8: Average BEP performance of FU by varying reflecting elements $N$ and RIS panels positions.

performance is significantly improved in MR-NOMA, as compared to RIS-NOMA and RSBT. Since more number of RIS panels near to BS or users reduce the path loss. BEP at low transmit power is $P_e^{\mathrm{NU}} \propto \exp\left(-\frac{N^6\pi^4 L_{1/2}^8\left(-K^2/K+1\right)\alpha_1 \mathrm{P}_t}{4(K+1)^4 P_1 N_0}\right)$, which has $N^6$ term in the exponent. Therefore, BEP decreases at low transmit power in MR-NOMA. In RSBT [76], the maximum received SNR path is selected from $L_1 \times L_2$ transmission paths. BEP performance of RSBT is inferior to the MR-NOMA due to its error probability is $P_e^{\mathrm{NU}} \propto \exp\left(-\frac{N^4\pi L_{1/2}^2\left(-K^2/K+1\right)\alpha_1 \mathrm{P}_t}{4(K+1)PN_0}\right)$ [76], where $P = d_{BR_p} d_{\mathrm{R}_p\mathrm{R}_q} d_{\mathrm{R}_{q,u}}$ denotes the distance between BS to RIS-p, RIS-p to RIS-q and RIS-q to users [76]. However, BEP performance of RSBT is better than RIS-NOMA and MR-NOMA *(Case-1)*, as observed in Figure 4.9.

Figure 4.10 highlights the impact of Rician factor $K$ for NU. Rician channel ($K \neq 0$) shows better BEP (around 20 dB at BER=$10^{-3}$) as compared to the Rayleigh channel ($K$=0) due to the presence of LoS component in the received signal. Therefore, LoS communication enhances system performance significantly in the MR-NOMA. Moreover, imperfect SIC (ISIC) is applied at NU and the maximum SNR is $\frac{Z_{\mathrm{NU}}\alpha_1 \mathrm{P}_t}{(N_0+\kappa\alpha_2 \mathrm{P}_t Z_{\mathrm{NU}})}$, where $\kappa$ denotes the imperfection in SIC. The value of $\kappa = 0$ indicates

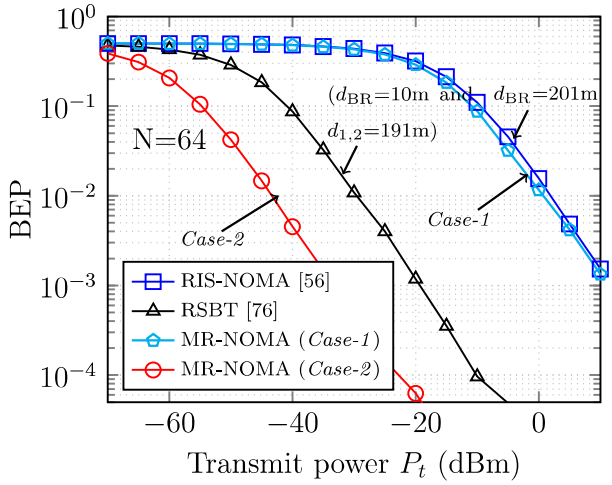


FIGURE 4.9: Comparison among the proposed MR-NOMA, R-NOMA and RSBT systems.

the perfect SIC. ISIC ($\kappa \neq 0$) degrades BEP performance of NU due to interference, as observed in Figure 4.10.

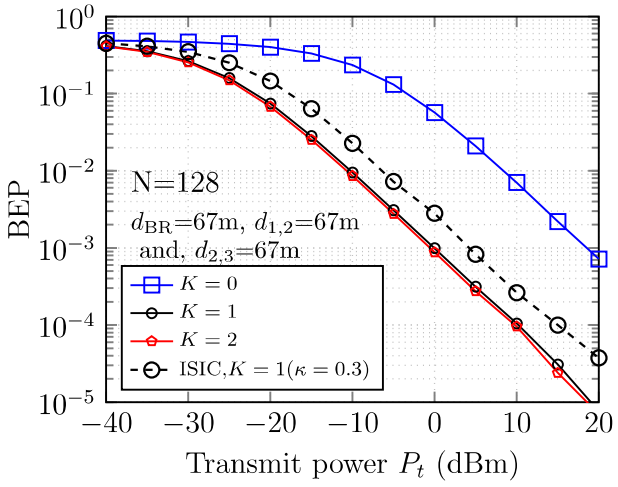


FIGURE 4.10: Average BEP performance of NU with perfect and imperfect SIC.

Figure 4.11 shows the average BEP of NU by varying the distance of RIS-2 from the RIS-1. It is observed that placing the RIS-2 near the RIS-1/RIS-3 yields the lowest

BEP; while placing it around the middle between the RIS-1 and RIS-3 leads to the highest BEP.

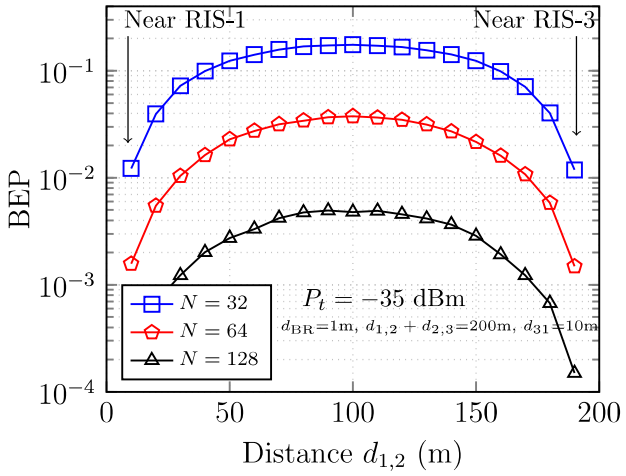


FIGURE 4.11: Average BEP performance of NU by varying RIS-2 panel distance $d_{1,2}$.

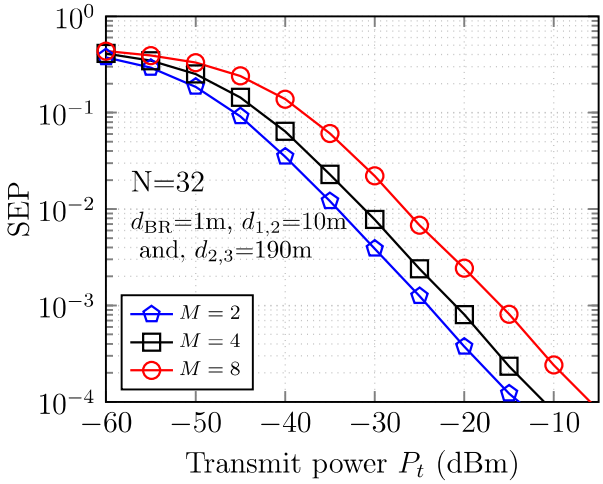


FIGURE 4.12: Average SEP performance of NU with varying modulation order $M$.

In Figure 4.11, RIS-1 and RIS-3 panels are fixed with BS and NU respectively. For better BEP performance, the RIS-2 is placed near to BS or NU. Since the received power is $P_r \propto N^6 \left(\frac{\lambda}{4\pi d_{\mathrm{BR}} d_{1,2} d_{2,3}}\right)^2$, which leads $P_r$ maximum when $d_{\mathrm{BR}}$& $d_{1,2}$ or $d_{1,2}$& $d_{2,3}$ are small. Further, Figure 4.12 shows the ASEP performance of NU in MR-NOMA system for modulation order $M = 2, 4, 8$. The SEP performance of NU

degraded as the modulation order $M$, increases because, $P_e^{\mathrm{NU}} \propto e^{(-\sin^2(\pi/M)N^6)}$. The results of the summary suggest that the performance of the proposed RIS-assisted system is improved by the deployment position of the RIS.

## 4.7 Summary

In this chapter, a centralized and distributed RIS-assisted NOMA for the downlink MISO system have been proposed. The BER and sum-rate performance of CDR-NOMA and DDR-NOMA system under the Rician flat fading channels have been analyzed and compared with conventional NOMA and OMA systems. The performances of system has been is improved by using SDR phase optimization technique, as observed in the above results. Further, it was observed that an imperfect SIC at NU has degraded the performance of the proposed system, and also observed that CDR-NOMA system performance is better than the DDR-NOMA system. As transmitting antennas and reflecting surfaces increase, BER and sum-rate performance improve in the proposed RIS-assisted NOMA system.

In the second phase of the chapter, a MR-NOMA system under Rician fading channels with a path-loss component was analyzed. The BEP expressions were derived for both NU and FU. The MR-NOMA system achieves better BEP at low transmit power as cascaded RISs create a LoS path between BS and users. Further, the performance of MR-NOMA was observed with reference to the position of RISs panels, channel model, and the number of reflecting surfaces. Deployment of RISs panels near to BS or users give better performance than other positions in the MR-NOMA, and the MR-NOMA yielded a superior performance over existing single RIS-NOMA and parallel MRIS.